BBA - Biomembranes 1860 (2018) 566–578

Contents lists available at ScienceDirect

BBA - Biomembranes

journal homepage: www.elsevier.com/locate/bbamem

Reconstitution of SNARE proteins into solid-supported lipid bilayer stacks and X-ray structure analysis

Yihui Xu[a], Jan Kuhlmann[b], Martha Brennich[c], Karlo Komorowski[a], Reinhard Jahn[d], Claudia Steinem[b], Tim Salditt[a,*]

[a] Institut für Röntgenphysik, Universität Göttingen, Friedrich-Hund-Platz 1, 37077 Göttingen, Germany
[b] Institut für Organische und Biomolekulare Chemie, Universität Göttingen, Tammannstraße 2, Göttingen 37077, Germany
[c] Structural Biology Group, European Synchrotron Radiation Facility, 71 Avenue des Martyrs, CS 90181, Grenoble 38042, France
[d] Department of Neurobiology, Max-Planck Institute for Biophysical Chemistry, Am Faßberg 11, Göttingen 37077, Germany

ARTICLE INFO

Keywords:
SNARE reconstitution
Supported lipid bilayer stack
Micelle and vesicle
SAXS
X-ray reflectivity
GISAXS

ABSTRACT

SNAREs are known as an important family of proteins mediating vesicle fusion. For various biophysical studies, they have been reconstituted into supported single bilayers via proteoliposome adsorption and rupture. In this study we extended this method to the reconstitution of SNAREs into supported multilamellar lipid membranes, i.e. oriented multibilayer stacks, as an ideal model system for X-ray structure analysis (X-ray reflectivity and diffraction). The reconstitution was implemented through a pathway of proteomicelle, proteoliposome and multibilayer. To monitor the structural evolution in each step, we used small-angle X-ray scattering for the proteomicelles and proteoliposomes, followed by X-ray reflectivity and grazing-incidence small-angle scattering for the multibilayers. Results show that SNAREs can be successfully reconstituted into supported multibilayers, with high enough orientational alignment for the application of surface sensitive X-ray characterizations. Based on this protocol, we then investigated the effect of SNAREs on the structure and phase diagram of the lipid membranes. Beyond this application, this reconstitution protocol could also be useful for X-ray analysis of many further membrane proteins.

1. Introduction

N-ethylmaleimide-sensitive factor attachment protein receptors (SNAREs) have been identified as a family of proteins which promote vesicle fusion. They mediate almost every individual trafficking step of the secretory pathway [1]. Although there are some other SNAREs and non-SNARE proteins involved in synaptic vesicle fusion, its driving force for the actual merger mainly originates from syntaxin (Syx) and SNAP25 which locate on the presynaptic plasma membrane, and synaptobrevin (Syb) which anchors itself in the synaptic vesicle membrane [2]. The Syx/SNAP25 complex and Syb bind with high affinity and together form a 4-helix bundle from the N-terminal to the C-terminal in a zipper like fashion [3]. It is commonly believed that this self-assembly supplies enough energy to overcome the repulsion between opposing membranes, pulls them into close contact and thus facilitates fusion [1,4].

To gain a clear insight into complicated SNARE-SNARE and SNARE-lipid interactions, model lipid membranes can be used and are amenable to structural characterizations, in particular to X-ray and neutron scattering [5]. Various model membrane systems have been developed ranging from black lipid membranes [6], vesicles [7], nanodiscs [8] and supported lipid bilayers [9,10]. For scattering studies, one can choose between several different scattering geometries and sample preparation methods, depending on the experimental constraints and the information required. Small-angle X-ray scattering (SAXS) of either unilamellar or multilamellar vesicles [11,12], can be used to deduce the bilayer electron density profiles from least-square fitting of the form factor.

The classical SAXS characterization is limited by the loss of structural information inherent in powder averaging. Provided suitable preparation techniques for highly aligned membranes, reflectivity and grazing incidence small-angle scattering (GISAXS) circumvent this loss of information. In these interface sensitive scattering techniques, the momentum transfer parallel ($q_{\parallel}$) and perpendicular (q_z) to the surface of the membranes can be well distinguished. Furthermore, the scattering volume can be precisely tuned by the angle of incidence α. To this end, the membrane mosaicity as quantified by the tilt distribution of membrane normal vectors ω, has to be smaller than the critical angle α_c of total external X-ray reflection. Preparation of such oriented single

* Corresponding author.
E-mail address: tsaldit@gwdg.de (T. Salditt).

https://doi.org/10.1016/j.bbamem.2017.10.023
Received 21 June 2017; Received in revised form 1 October 2017; Accepted 24 October 2017

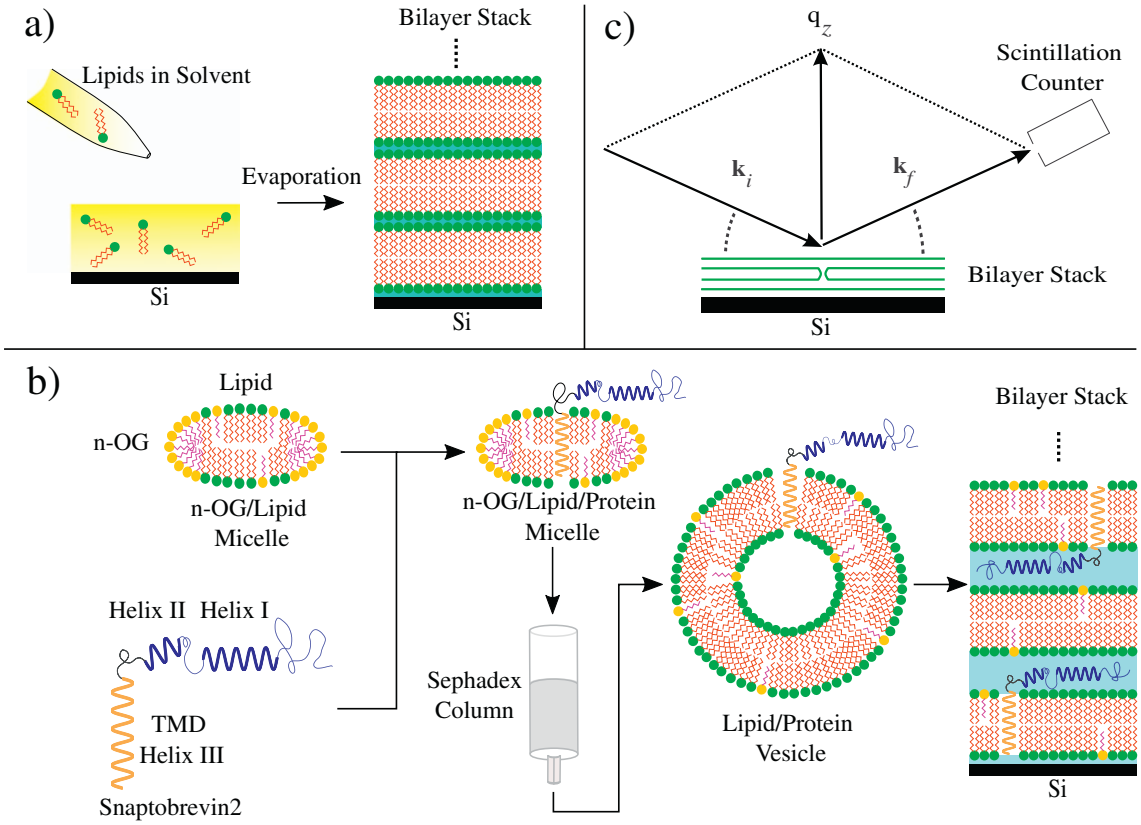

Fig. 1. (a) Cartoon of the conventional spreading organic solution (sOS) method. (b) Cartoon flow chart of the spreading vesicle suspension (sVS) method. (c) Sketch of the reflectivity experiment used as one of the characterization approaches of the multilamellar bilayers.

bilayers [13] or bilayer stacks [14,15] then offers the opportunity to map the two-dimensional reciprocal space. X-ray reflectivity, which probes the structure factor along q_z typically offers strong signal, and thus provides the electron density profile ρ(z) as well as the inter-bilayer correlations down to the Angstrom scale [16,17]. Contrarily, lateral correlations and structure in particular regarding the proteins which can be monitored by GISAXS, exhibit much weaker signal. While synchrotron radiation is brilliant enough to still pick up the diffraction signal of a single monolayer or bilayer, it is often advisable to amplify the diffraction signal by increasing the number of bilayers *N*. Aside from the higher signal, a further advantage of studying membrane proteins using bilayer stacks (i.e. multibilayers) is that structural alterations and artifacts induced by the substrate surface can be significantly reduced [18]. Adding a soft cushion or tethering can overcome this problem also for single supported bilayers [19], but at the expense of extra complexity and additional structural parameters.

However, membrane proteins including SNAREs cannot be reconstituted into oriented bilayer stacks with the rather convenient and most frequently used solvent method which achieves film deposition by spreading organic solution (sOS) onto solid-supports (Fig. 1a) [20,21]. In the sOS protocol, the lipid molecules gradually self-assemble into lipid bilayers during solvent evaporation, and in the end form well-aligned, homogeneous bilayer stacks on the substrates. Although the use of organic solvent is not a concern and even desired for optimized mixing in many lipid-peptide systems, it is prohibitive for membrane proteins. Alternatively, membrane proteins (e.g. glycophorin, porin and bacteriorhodopsin [22]) can be reconstituted into lipid bilayer stacks by depositing proteoliposome suspensions onto solid-supports. This approach is similar to the deposition of supported single bilayers with vesicle suspensions [23], which has already been extensively applied to the reconstitution of SNAREs [24,25]. The main difference between these two is that for single bilayers only a single layer of vesicles adsorb onto the solid-supports and slowly rupture into single bilayers, while for bilayer stacks bulk vesicle suspensions are forced to dry and to form multibilayers during water evaporation. A related solvent-free approach, which did not include reconstituted proteins, was presented by Kucerka et al. [26].

In this work we show how reconstituted SNAREs can be incorporated into oriented lipid bilayer stacks enabling X-ray analysis without powder averaging. This is required to unambiguously identify the stalk structures from the two-dimensional GISAXS diffraction pattern, as previously shown for pure lipid systems [27,28]. A first goal is then to verify the structural integrity of the multi-bilayer stacks, and to quantify how the inter-membrane distance, i.e. the lamellar repeat distance *d*, as well as the lamellar ordering and electron density changes with protein reconstitution. Note that the X-ray measurements are dominated by the indirect collective response of the bilayer to protein insertion, not by proteins directly. Another important goal which motivates this study is to find out how the phase diagram changes in the presence of SNAREs, and whether reconstituted SNAREs promote the equilibrium stalk phase, i.e. are able to lower the critical osmotic pressure at which the phase appears. Finally, a long term goal is the reconstruction of the three-dimensional electron density distribution ρ(**r**) of model membranes containing SNAREs in the rhombohedral (*R*) phase.

To obtain oriented membrane stacks with reconstituted SNAREs, vesicles containing v- and t-SNAREs were first separately prepared by eluting SNARE-containing micelles through size-exclusion columns [29], and then spread onto Si substrates, as shown in Fig. 1b. This SNARE reconstitution protocol was carefully monitored and validated by verifying the structural transitions in each step (i.e. proteomicelle to proteoliposome to multibilayer). SNARE-reconstituted proteomicelles and proteoliposomes were studied by SAXS to reveal the effective structural changes. The supported multibilayers were characterized by X-ray reflectivity and GISAXS, which together provided a detailed view of the effects of SNARE reconstitution on the multibilayers. This

solvent-free method, denoted as spreading-vesicle-suspension (sVS), is introduced in detail below, followed by the description of X-ray analysis and the presentation of the phase diagram results.

2. Materials and methods

2.1. Protein expression and purification

The protein expression and purification were described in detail in [30,31]. Briefly, SNAREs from *Rattus norvegicus* were cloned with the *pET28a* vector in *E-Coli* (strain BL21(DE3)). Subsequently the expressed and isolated SNAREs were purified by Ni-NTA agarose and ion exchange chromatography on MonoQ or MonoS columns (GE Healthcare). His6-tags were cleaved by thrombin digest overnight prior to ion exchange chromatography. Proteins with transmembrane domains (TMD) were handled in the presence of 16 mM CHAPS. The full length Syb (residues 1-116), one of the natural vesicular SNARE components, was directly used. The SNARE motif and transmembrane segment of syntaxin-1A (residues 183-288), SNAP-25A (residues 1-206, with all cysteines replaced by serines), and the C-terminal soluble segment of synaptobrevin 2 (residues 49-96) were assembled into the ΔN acceptor complex (hereinafter referred to in short as ΔN complex or ΔN) overnight at 4 °C and further purified by MonoQ ion exchange chromatography in the presence of 16 mM CHAPS. Here ΔN served as the t-SNARE complex, due to its high assembly rate with Syb compared to the "unproductive" 2:1 complex of syntaxin and SNAP25 [29,32].

2.2. Preparation of proteoliposomes

The preparation of proteoliposomes for later deposition [29,30] is sketched in Fig. 1b, where Syb is used as an example to illustrate how SNAREs anchor in various aggregates, from micelles to vesicles, and to multibilayers. Proteoliposomes reconstituted with SNAREs were first prepared by size exclusion chromatography [33]. Four lipids were used in this study: 1,2-dioleoyl-*sn*-glycero-3-phosphocholine (DOPC or PC), 1,2-dioleoyl-*sn*-glycero-3-phosphoethanolamine (DOPE or PE), 1,2-dioleoyl-*sn*-glycero-3-phospho-L-serine (DOPS or PS) and Cholesterol (Chol). 1 mg of either PC-PE 4:1 or PC-PE-PS-Chol 5:2:2:1 *mol/mol* was dissolved in chloroform/(2,2,2)-trifluoroethanol mixture (1:1 *vol/vol*) and dried by nitrogen flow for 1 h. The film was then stored in vacuum for 2 h to fully remove the organic solvents. 1.8 mg n-octyl-β-D-glucoside (n-OG) was added to 50 μL buffer solution composed of 20 mM 4-(2-hydroxyethyl)-1-piperazineethanesulfonic acid (HEPES), 100 mM KCl and 1 mM dithiothreitol (DTT), and then used to re-dissolve the dry lipid film. The n-OG concentration (~120 mM) was much higher than its CMC (25 mM) so that detergent/lipid mixed micelles were formed [34]. Afterwards, ΔN or Syb suspension containing 1% CHAPS was added until the protein/lipid ratio reached 1:500. The resulting suspension was incubated on ice for 30 min in order to form detergent/lipid/protein mixed micelles. The remaining detergent was removed by a Sephadex G-25 size-exclusion column (Illustra NAP-25, GE Healthcare) equilibrated with the reconstitution buffer, and salt was removed by another Sephadex G-25 column equilibrated with ultrapure water. During this process, vesicles were formed as n-OG was removed. The collected vesicle suspension was concentrated from 1000 to 100 μL by a concentrator (Concentrator plus, Eppendorf). Finally, suspensions of proteoliposomes reconstituted with either ΔN or Syb were gently mixed (50 μL each) and incubated at room temperature for 30 min, allowing for possible fusion. In addition a control sample without detergent was prepared by sonicating the PC-PE-PS-Chol lipid film together with ultrapure water. All micelles and vesicles were characterized by SAXS to confirm their structures and to determine their structural parameters.

2.3. Preparation of lipid bilayer stacks

Four different lipid mixtures (PC-PE, PC-Chol, PC-PE-Chol and PC-PE-PS-Chol) were tested for the sVS preparation of multibilayers. All of them yielded multibilayers with sufficient orientation and long-range order for X-ray investigations. PC-PE was selected as the primary lipid composition for multibilayer deposition based on our previous experience that PC-PE mixtures form highly oriented bilayer stacks with rhombohedral (*R*) phases already forming at relatively mild dehydration [28,35].

Polished silicon wafers (Silchem) cut to $10 \times 15\ mm^2$ were ultrasonic-cleaned by methanol and ultrapure water, and then surface treated by a plasma cleaner (PDC-002, Harrick) under a constant O_2 flow for 10 min to achieve a highly hydrophilic SiO_2 layer. Prior to deposition, the proteoliposome suspension containing ΔN and Syb was prepared as described above. The resulting suspension was first pipetted onto the wafer, which was then brought into a vacuum desiccator, followed by over-night evacuation to thoroughly remove H_2O, yielding oriented dry multibilayers. The pure lipid multibilayer and the multibilayer containing only ΔN were prepared in the same way, to serve as control samples. The supported lipid multibilayers were then ready for the characterization by X-ray reflectivity and grazing-incidence small-angle scattering (GISAXS).

In addition, pure lipid multibilayers were also prepared by conventional spreading organic solutions (sOS) to serve as control samples and benchmarks for the sVS samples. 1 mg lipid mixture was solved by 100 μL chloroform/(2,2,2)-trifluoroethanol (1:1 *vol/vol*). The stock solution was directly pipetted onto the Si substrate. The wafer carrying the lipid solution was first kept in the fume hood for 2 h to form oriented bilayer stacks and then in vacuum for overnight to remove all solvents.

2.4. Small-angle X-ray scattering (SAXS) on proteomicelles and proteoliposomes

SAXS investigation of proteomicelles and proteoliposomes was carried out at the bioSAXS beamline (BM29) of the European Synchrotron Radiation Facility (ESRF). The beam was monochromatized by a double multilayer monochromator and defined to $700 \times 700\ \mu m^2$ at the sample capillary. The photon energy was set to 12.5 keV. A pixel detector (Pilatus 1M, Dectris) with 981×1043 pixels and $172 \times 172\ \mu m^2$ pixel size was mounted 2.867 m away from the capillary. Sample suspensions and buffer solutions were first pre-pipetted into the wells of the automatic sample changer before they were delivered into the capillary for exposure. For each sample 10 frames of 1 s were collected with the local software BsxCuBE [36], and azimuthally integrated to 1d profiles by EDNA-based data processing pipeline, which then disposed the profiles with radiation damage, averaged the remaining ones, and subtracted the best buffer data, yielding scattering curves of the investigated aggregates [37,38].

The micelle SAXS data was fitted by the two-component ellipsoid model [39,40], in which the alkyl chains are considered as the less electron-dense inner core and the headgroups as the outer shell with a higher electron density, as sketched in Fig. 2c. The inner core is parameterized by the inner electron density ρ_1, the polar radius a and the equatorial radius b, and the outer shell by the outer electron density ρ_2, the headgroup thickness t_a and t_b. Here the electron density of the buffer solution (ρ_s) is considered to be close to the value of pure water (0.334 e/Å^3). The scattering intensity is then given by:

$$I(q) = s < F(q)^2 > + f = s \int_0^1 (3V_1(\rho_1 - \rho_2)J_1(u_1)/u_1 + 3(V_1 + V_2)(\rho_2 - \rho_s)J_1(u_2)/u_2)^2 dx + f, \quad (1)$$

with $u_1 = q\ (a^2x^2 + b^2(1-x^2))^{1/2}$, $u_2 = q\ ((a+t_a)^2x^2 + (b+t_b)^2(1-x^2))^{1/2}$, the inner volume $V_1 = 4/3\pi ab^2$, and the total volume $V_1 + V_2 = 4/3\pi(a+t_a)(b+t_b)^2$. $F(q)$ is the micelle form factor. s and f are the scaling factor and the linear background. J_1 denotes the first-order spherical Bessel function. The fitting was performed using the *lsqnonlin* routine in the Optimization Toolbox of MATLAB

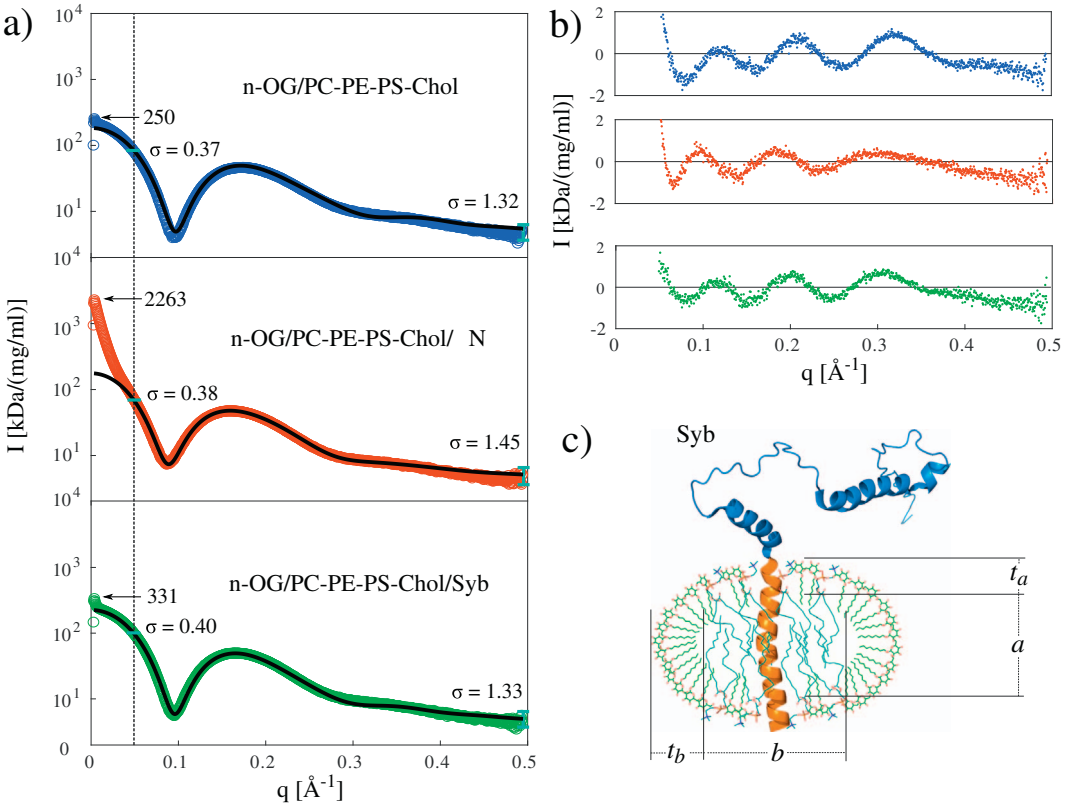

Fig. 2. (a) SAXS curves (colored circles) and their fits (black lines) of (i) n-OG/PC-PE-PS-Chol, (ii) n-OG/PC-PE-PS-Chol/ΔN, and (iii) n-OG/PC-PE-PS-Chol/Syb micelles, plotted on a logarithmic scale. The micelle mass concentration (total surfactant and lipid) is ~36 mg/mL. Data in the q range of 0.050–0.495 Å^{-1} has been fitted, as indicated by the vertical dashed line. The from factor values for $q \to 0$ are marked by arrows. By virtue of the instrument's calibration in absolute units, scattering intensity can be expressed in terms of (effective) molar mass of an equivalent protein solution, if the concentration c of the scatterers is known. The experimental errors of the first and last fitted data points are plotted in cyan. (b) Residuals of the two-component ellipsoid fits, corresponding to the fits shown in (a). (c) 2d sketch of the possible molecular arrangement of the n-OG/PC-PE-PS-Chol/Syb proteomicelle, using the micelle size determined by fitting (Table 1a) and PDB molecular structures (PDB ID for Syb: "2KOG"). The sketch is assembled "by hand" using PyMOL.

(MathWorks Inc.).

The vesicle SAXS data was fitted by the symmetric flat bilayer model (reasoning see Appendix D), in which the vesicle bilayer is treated as effectively flat and symmetric [41,42]. Three Gaussian shells were used to model the two headgroup regions (the 1st and 3rd shells) and the alkyl region (the 2nd shell) of the bilayer. The scattering intensity [43] was calculated according to

$$I(q) = s < F(q)^2 > + f = sq^{-2} \sum_{k,k'}^{3} \rho_k \rho_{k'} \sigma_k \sigma_{k'} exp[-q^2(\sigma_k^2 + \sigma_{k'}^2)/2] \times cos[q(\varepsilon_k - \varepsilon_{k'})] + f, \quad (2)$$

where s and f are again the scaling factor and the linear background. Here $F(q)$ is the vesicle form factor. ρ_k and σ_k are the maximum electron density contrast in arbitrary units and the standard deviation of the kth Gaussian shell, respectively. The maximum electron density contrast between the headgroup and alkyl chain ρ_2 is set to -1. The position of the $\varepsilon_k$kth Gaussian function is taken with respect to the bilayer mid-plane. The total membrane thickness d_{hh} is defined by $d_{hh} = |\varepsilon_1 - \varepsilon_3|$. Under the symmetry condition, $\rho_1 = \rho_3, \sigma_1 = \sigma_3, \varepsilon_1 = -\varepsilon_3$, and hence $d_{hh} = 2|\varepsilon_1|$. The fitting of vesicle SAXS curves was also performed using the *lsqnonlin* routine.

2.5. X-ray reflectivity

X-ray reflectivity characterization was carried out at the same home-built laboratory diffractometer as used previously [28,35]. The Cu Kα (λ = 1.54 Å, E = 8.048 keV) beam was generated by a long fine focus X-ray tube (GE-Seifert) operating at U = 35 kV and I = 40 mA, collimated and monochromatized by a parabolic multilayer Goebel mirror, and automatically attenuated by a motorized filter wheel. A set of entrance slits were placed before the sample to define the beam size to be 0.8 mm horizontally and 3 mm vertically. The samples were mounted vertically in a sealed chamber, where both the relative humidities (RHs) and temperatures were precisely controlled [44]. Reflectivity scans with coupled $\theta/2\theta$ were recorded by a fast scintillation counter (Cyberstar, Oxford-Danfysik), with a resolution of $\Delta\theta = 0.01°$ and 2 s counting time at each $\theta/2\theta$ position. The incidence angle θ was converted into perpendicular momentum transfer with $q_z = 4\pi\sin\theta/\lambda$. The intensities were plotted against q_z, yielding a series of reflectivity curves at 22 ° C and various RHs.

The electron density profiles (EDPs) along the membrane normal (the z direction) were reconstructed from the reflectivity curves using the Fourier synthesis method [35,45], where

$$\rho(z) = \sum_n \nu_n \sqrt{F_n} \cos(q_n \cdot z). \quad (3)$$

ν_n and F_n are the phase and the scattering intensity of nth Bragg order, corrected for the Lorentz factor. Only the first five peaks were taken into consideration. The phase combination was manually set to $-1, -1, +1, -1, +1$ [35,44] to yield physically consistent EDPs.

The bilayer periodicity d was calculated using Bragg's Law $2d\sin\theta = n\lambda$, and averaged over observable Bragg peaks. Note that neither the first Bragg peak which was affected by the Fresnel reflectivity of the substrates, nor the last Bragg peak which was mostly too weak, were used in this calculation [46].

2.6. Grazing-incidence small-angle X-ray scattering (GISAXS)

GISAXS experiments of the multibilayers were carried out both at microdiffraction imaging beamline (ID01) of ESRF and at our in-house diffractometer. At ID01, the photon energy was set to 17.91 keV and the beam size at the sample was defined to 160 × 20 μm^2. The beam was monochromatized by a Si (111) double crystal monochromator and attenuated by a 200 μm thick Mo attenuator. A Medipix TAA22PC pixel detector with 516 × 516 pixels and 55 × 55 μm^2 pixel size was mounted on the detector arm of the six-circle diffractometer at a distance of 178.59 mm behind the samples. The primary beam, the reflected beam and the first Bragg peaks were attenuated by a rectangular Si beamstop right in front of the detector. The wafers were placed horizontally on the bottom of the RH chamber. Each diffraction image was recorded with 10 s exposure time. The possibility of radiation damage was eliminated by checking the consistency of adjacent exposures. Only lamellar hydration conditions (RH 95% and 90%) were applied to the multibilayers at ID01.

At our in-house diffractometer, a Cu Kα ($\lambda = 1.54$ Å, $E = 8.048$ keV) beam was produced by a rotating anode generator (MicroMax-007 HF, Rigaku) operating at $U = 40$ kV and $I = 30$ mA. The beam was paralleled and monochromatized by a parabolic multilayer Goebel mirror and defined to 1 × 1 mm^2 size by the entrance slits. A square Si beamstop was used to attenuate the bright primary beam. A Pilatus 100 K pixel detector (DECTRIS) with 487 × 195 pixels and 172 × 172 μm^2 pixel size was mounted 200 mm behind the sample. Each image was recorded with 1000 s exposure time. Exposures were conducted at various hydration conditions (RH 50–90 % at 2% intervals) to inspect the phase behaviors of the multibilayers, particularly in the presence of SNAREs.

3. Results and discussion

3.1. SAXS results of the proteomicelles

Fig. 2a shows the SAXS data (colored circles) of (i) n-OG/PC-PE-PS-Chol, (ii) n-OG/PC-PE-PS-Chol/ΔN, and (iii) n-OG/PC-PE-PS-Chol/Syb micelles. All curves exhibit the typical functional form of micelles [47], with only small systematic changes except for $I(q \to 0)$, where the curve corresponding to the ΔN-containing micelles exceeds the value of the Syb-containing micelles by a factor of about 7 and that of the protein-free micelles by a factor of 9. This change is indicative of a certain degree of protein aggregation, as we discuss further below. As a further model-free parameter, the dominant head group to head group length L can be derived from the 2nd peak position [40] without any model fit. All mixtures showed similar L (36.61–40.02 Å), with the SNARE-containing micelle solution being slightly larger (40.02 Å for ΔN and 37.85 Å for Syb) than the pure n-OG/lipid micelles (36.61 Å). These parameters were verified by a full q-range fit based on the two-component ellipsoid model (black lines) [39], which introduces more micelle structural parameters. All fitting parameters are summarized in Table 1a. The model fits describe the experimental data sufficiently well in the fitted region (q = 0.050-0.495 Å^{-1}). Note that 0.05 Å^{-1} was chosen as the fitting window (low-q cutoff) in order to exclude the scattering signal of proteins, which was not incorporated in the micelle model. This is justified by the observation that for $q \leq 0.05$ Å^{-1} the curve of the nOG/lipid/ΔN proteomicelles deviates strongly from that of the protein-free micelles, while its functional form is fairly well captured by the micelle model for $q \geq 0.05$ Å^{-1}. Note also that (incoherent) subtraction of the pure nOG/lipid micelles data from that of proteomicelles would not simply yield the SAXS signal of SNAREs alone, since the scattering from the micelle and reconstituted protein interfere. We can therefore not strictly apply the subtraction presented in [48]. The remaining systematic discrepancies observed in the residuals plotted in Fig. 2b show, however, that the two shell model might be over-simplified.

Parameters in Table 1a indicate that all mixed micelles adopt an oblate shape ($a < b$), in agreement with previous observations that n-OG/PC micelles are “flattened” [49,50]. The geometrical parameters, namely the semi-axis length a and b, the shell thickness t_a and t_b, increase only slightly for the SNARE-containing suspensions, in good agreement with the model-free parameter L above.

In order to interpret these structural results, we must keep in mind that the SAXS corresponds to an ensemble, i.e. an average over SNARE-containing and SNARE-free micelles within the illuminated volume. According to the estimation in Appendix A based on the stoichiometry used in the reconstitution, we expect only ~ 9% of the micelles to contain a SNARE protein. The SAXS signal is thus dominated by the protein-free micelles, which explains that all curves give very similar micelle parameters. However, larger aggregations must be present in the ΔN-containing solution. To see this, we first compute an upper bound for the total mass of a SNARE-containing micelle. From the fitted geometrical form factors of the micelles and the known composition and stoichiometry of surfactants and lipids, we obtain values in the range of 70–80 kDa. We add it to the molecular masses of the protein $M_{\Delta N} = 40.993$ kDa, or $M_{Syb} = 12.69$ kDa, respectively, and compare this sum to the molecular mass extracted from $I(q \to 0)$ of the calibrated scattering intensity. Note that the molecular masses of the instrument apply to protein solutions, assuming a protein mass density of $\rho_P = 1.35$ g/cm^3 [51]. Therefore, $I(q \to 0) = 2263$ kDa/(mg/ml) of the ΔN curve must be scaled with the corresponding contrast ratio (micelle-to-water/protein-to-water). Taking this into account along with the concentration $c \simeq 36$ mg/ml, we get values well in excess of 120 kDa, which we consider evidence of aggregation. At the same time, we presume that not all ΔN-containing micelles aggregate based on the clarity of the solution. Finally, we note that in view of problems

Table 1
(a) Fitting results of the SAXS data of (i) n-OG/PC-PE-PS-Chol, (ii) n-OG/PC-PE-PS-Chol/ΔN and (iii) n-OG/PC-PE-PS-Chol/Syb micelles. (b) Fitting results of the SAXS data of (i) PC-PE-PS-Chol vesicles prepared by sonication, (ii) PC-PE-PS-Chol, (iii) PC-PE-PS-Chol/ΔN, (iv) PC-PE-PS-Chol/Syb and (v) PC-PE-PS-Chol/ΔN + Syb vesicles prepared by size-exclusion. Here $d_{hh} = 2|\varepsilon_1|$.

(a) 2-component ellipsoid fitting results of the micelle SAXS data

Samples	a [Å]	b [Å]	ρ_1 [e/Å^3]	ρ_2 [e/Å^3]	t_a [Å]	t_b [Å]	χ^2_{red}
n-OG/PC-PE-PS-Chol	11.66 ± 0.22	28.65 ± 0.34	0.24 ± 0.00	0.46 ± 0.01	11.09 ± 0.41	3.38 ± 0.17	22.22
n-OG/PC-PE-PS-Chol/ΔN	11.97 ± 0.11	36.82 ± 1.29	0.24 ± 0.00	0.47 ± 0.01	12.64 ± 0.26	5.00 ± 0.40	8.56
n-OG/PC-PE-PS-Chol/Syb	11.87 ± 0.13	31.40 ± 0.43	0.25 ± 0.00	0.47 ± 0.01	12.59 ± 0.27	2.71 ± 0.22	12.80

(b) Symmetric flat-bilayer fitting results of the vesicle SAXS data

Samples	$\lvert\varepsilon_1\rvert$ [Å]	σ_1 [Å]	σ_2 [Å]	ρ_1 [a.u.]	d_{hh} [Å]	χ^2_{red}
PC-PE-PS-Chol by sonication	18.76 ± 0.27	6.52 ± 0.32	11.28 ± 1.05	1.03 ± 0.03	37.52 ± 0.54	1.51
PC-PE-PS-Chol	18.04 ± 0.25	5.22 ± 0.36	10.50 ± 0.94	1.09 ± 0.03	36.08 ± 0.50	1.46
PC-PE-PS-Chol/ΔN	19.14 ± 0.18	4.21 ± 0.17	10.05 ± 0.94	1.09 ± 0.02	38.28 ± 0.36	1.50
PC-PE-PS-Chol/Syb	18.38 ± 0.19	5.51 ± 0.32	10.19 ± 0.66	1.05 ± 0.02	36.76 ± 0.38	1.41
PC-PE-PS-Chol/ΔN + Syb	18.93 ± 0.12	4.60 ± 0.14	9.64 ± 0.75	1.08 ± 0.02	37.86 ± 0.24	1.21

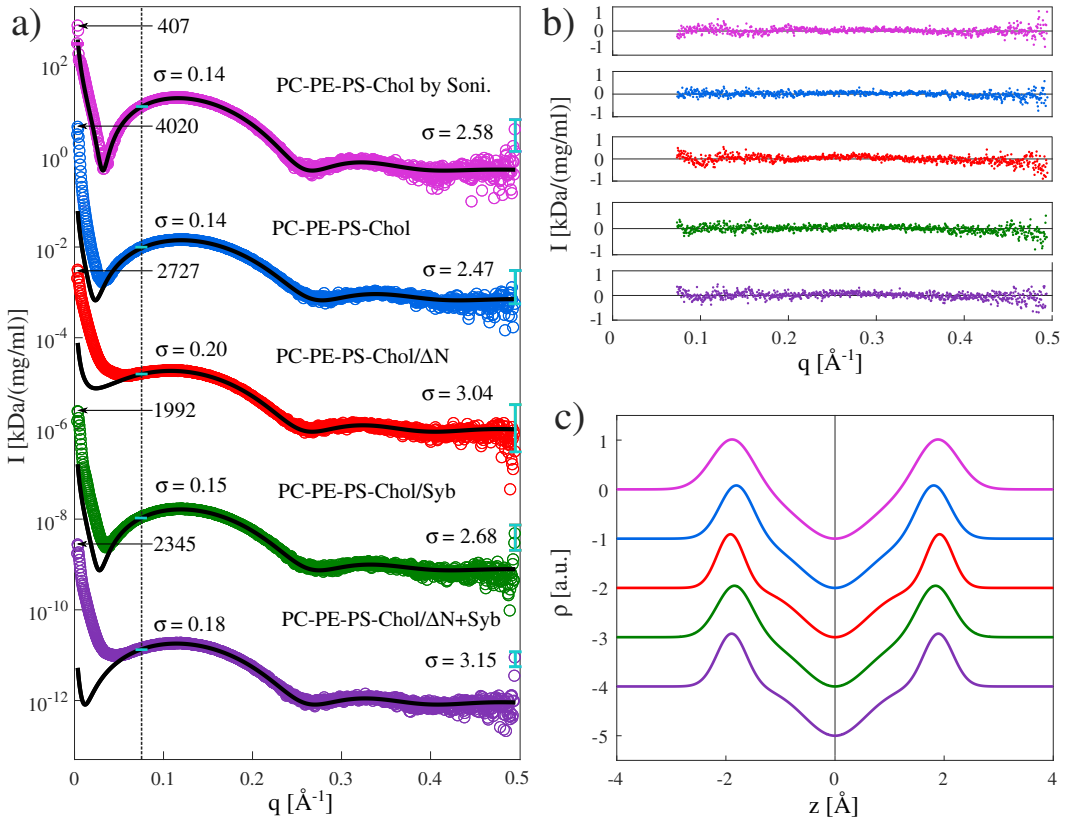

Fig. 3. (a) SAXS curves (colored circles) and their fits (black lines) of (i) PC-PE-PS-Chol vesicles prepared by sonication, (ii) PC-PE-PS-Chol, (iii) PC-PE-PS-Chol/ΔN, (iv) PC-PE-PS-Chol/Syb and (v) PC-PE-PS-Chol/ΔN + Syb vesicles prepared by size-exclusion. Both are plotted on a logarithmic scale and shifted for clarity. The mass concentration of the lipid is ~7 mg/mL. Data in the q range of 0.075–0.495 Å^{-1} is fitted, as indicated by the vertical dashed line. The intensities of $q \to 0$ are again marked by arrows. The experimental errors of the first and last fitted data points are plotted in cyan. (b) Corresponding residuals of the fits to the symmetric flat-bilayer model. (c) Electron density profiles reconstructed with the obtained fitting parameters in Table 1b.

associated with aggregation and averaging over inhomogeneous scatterers, the systematic discrepancies are not surprising, but since the residuals are comparable for all curves, we still conclude that the main limitation of this model is the over-simplistic description of the micelles. In particular, the present mixed micelles cannot be characterized well by a uniform headgroup, as they incorporate both lipids and detergents especially in the highly mixed regions. The two-component ellipsoid model may therefore fail to properly fit the data, accentuating the usual deficiencies of the model in the high q range [39,52]. Nonetheless, the small averaged expansion of the micelles does indicate a measurable response of the system to SNARE reconstitution into the n-OG/lipid micelles, so that the SNARE reconstitution into vesicles can be subsequently performed.

3.2. SAXS results of the proteoliposomes

Fig. 3a shows the SAXS data (colored circles) and the fits (black lines) of (i) PC-PE-PS-Chol vesicles prepared by sonication, (ii) PC-PE-PS-Chol, (iii) PC-PE-PS-Chol/ΔN, (iv) PC-PE-PS-Chol/Syb and (v) PC-PE-PS-Chol/ΔN + Syb vesicles prepared by size-exclusion. The fitting results are summarized in Table 1b. They show that bilayer thicknesses d_{hh} of vesicles vary considerably with the preparation methods and the compositions. Firstly pure PC-PE-PS-Chol vesicle bilayer prepared by sonication (d_{hh} = 37.52 Å) is thicker than the one prepared by size-exclusion (d_{hh} = 36.08 Å). As they have the same lipid composition, the only appropriate explanation is that there was fairly abundant detergent (mainly n-OG) left in the bilayers, which inserted into the lipid bilayers in a wedge-like fashion [53] and lead to bilayer thinning [54]. Secondly for sVS vesicles of PC-PE-PS-Chol/ΔN (d_{hh} = 38.28 Å) and PC-PE-PS-Chol/Syb (d_{hh} = 36.76 Å), d_{hh} is increased with respect to PC-PE-PS-Chol (protein-free control). This is somewhat similar to the observed swelling of micelles discussed above. In contrast to the micelles, however, the protein copy number of a vesicle is much larger than one, in fact for 100% reconstitution efficiency we expect 44 proteins for a R = 30 nm vesicle (see Appendices B and C). Given the still low protein-to-lipid ratio P/L = 0.002, we cannot expect however to see a large contribution of the "protein shell" around the bilayer. For this reason, it is plausible that the electron densities reflect mainly the small changes which the protein reconstitution brings to the lipid matrix, i.e. proteins are sensed only indirectly at this P/L. For comparison, Fig. 3c shows the electron density profiles (EDPs) of all 5 types of vesicle bilayers reconstructed with the fitting parameters in Table 1b. They show that the bilayer structure is not significantly altered by SNARE reconstitution, apart from the minor membrane thickening. Lastly, almost all fitting parameters of the mixed vesicles (PC-PE-PS-Chol/ΔN + Syb) are approximately the average of the non-mixed ones. It is likely that full fusion brings about no observable changes to the SAXS results, as long as the flat bilayer model is used to describe the data, i.e. as long as we are insensitive to the vesicle radius. However, we should be able to detect characteristic signals from docking and hemifusion. Since the SAXS curve of the mixed SNARE vesicles (purple) is roughly the average of the curves of single SNARE vesicles (red and green), we cannot identify any such effect.

Finally, we address a possible aggregation of the ΔN-containing vesicles, since the micelles exhibited such an aggregation. Indeed, again there is also a minor contribution from larger aggregates, specific to ΔN-containing vesicle, as evidenced by dynamic light scattering (Appendix B). The majority of vesicles is however in an unaggregated fraction with radii in the expected size range around $R_0 \approx$ 30 nm.

SAXS results of various micelles and vesicles together support a

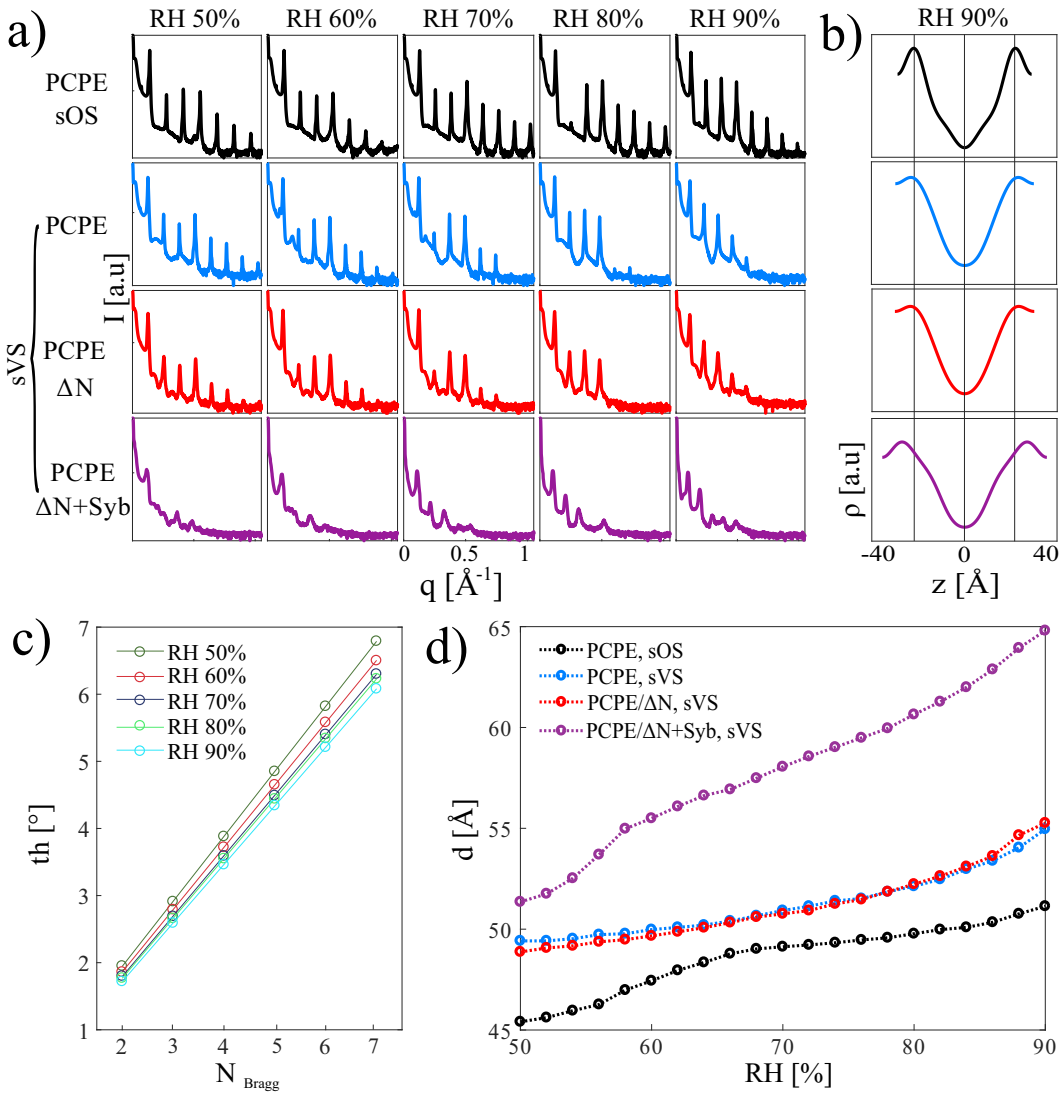

Fig. 4. (a) Reflectivity curves of various PC-PE 4:1 multibilayers at selected hydration conditions. Curves are plotted on logarithm scale in the q range of 0–1.05 Å^{-1}. (b) Electron density profiles reconstructed from the reflectivity curves of RH 90%. (c) Bragg peak positions (circles) and the fits (solid lines) of the reflectivity curves of PC-PE 4:1 prepared by sOS used for the determination of bilayer periodicity d. The first and last Bragg peaks are not used [46]. (d) d plotted as a function of RH. All circles represent performed measurements and connected by dashed lines for better visual inspection.

simple picture of protein reconstitution. The SNAREs anchor themselves into the host aggregates via the TMDs, leading to minor structural modifications in the detergent and lipid assembly. This knowledge is a prerequisite for the following discussion of multibilayers, as pronounced geometrical alterations of the vesicles would possibly also have an effect on the subsequent formation of multibilayers.

3.3. X-ray reflectivity

Fig. 4a shows the reflectivity curves of (i) pure PC-PE 4:1 multibilayer prepared by sOS, (ii) pure PC-PE 4:1, (iii) PC-PE/ΔN and (iv) PC-PE/ΔN + Syb multibilayers prepared by sVS, at selected hydration conditions. First we compare the reflectivity curves of pure PC-PE prepared with both methods: A series of Bragg peaks could be observed at all measured RHs on both membranes. For the PC-PE multibilayer prepared by sOS (black), at least 8 Bragg orders (some not shown in this q range) consistently appear for all measured hydration conditions. While for the PC-PE membrane prepared by sVS (blue), a fewer number of Bragg orders (5 at RH 90%, up to 8 at RH 50%) could be recorded. Such a decrease in Bragg order numbers indicates more static defects and a reduced long-range order, even in the absence of SNAREs. In the sOS preparation, lipid molecules move freely in the organic solution and bilayers can therefore find lower energy mesoscopic states more easily during solvent evaporation. Contrarily, lipid bilayers in the sVS preparation are deposited onto the wafers via vesicle adsorption and rupture. Inevitably, there can be a certain amount of partial ruptures resulting in more bilayer defects [55]. Moreover, some weak new peaks show up in the sVS curves besides the regular Bragg orders (e.g. at RH 60%). They will be further investigated later by GI-SAXS, which is more suitable for phase determinations. On the positive side however, 5-8 Bragg orders is already a sign of high lamellar order. With them we could already perform EDP reconstitution by means of Fourier synthesis [56]. It seems that despite the existence of unruptured vesicles, the sVS preparation is still able to facilitate multibilayers with high long-range order. Next we compare the reflectivity curves of the different samples prepared with the sVS method. The curves of sVS multibilayer with ΔN (red) look highly alike the pure lipid sVS multibilayer. Similar to the pure PC-PE bilayer stacks prepared by sVS, the PC-PE/ΔN membrane also exhibits high long-range order. In the SAXS section above, we have determined that single SNAREs solely result in a structural modification to their host aggregates. It seems to continue to be the case for the supported bilayer stacks. The multibilayer with

mixed ΔN and Syb (purple) however shows a completely different lineshape from the other two sVS multibilayers, with merely 5 Bragg peaks observable. We have learned from the SAXS results that in the suspension state the two SNARE do not strongly associate with each other. It seems that they do in the multibilayer state, where bilayers are forced into close contact [57]. In the presence of both ΔN and Syb, the bilayer could dock, hemifuse or fuse, yielding various vesicle geometries and sizes [30]. As a result, more defects appear and the multibilayer long-range order decreases.

Fig. 4b shows the EDPs reconstructed with the reflectivity curves at RH 90%. It is only performed at higher RHs where clean lamellar peaks can be obtained for all curves, with the EDPs of RH 90% shown as an example. Firstly, the EDP lineshapes of the sVS multibilayers (blue, red and purple) appear similar to each other regardless of SNAREs, but distinct from the lineshape of the sOS multibilayer (black). This observation indicates a lower electron density contrast between the water layer and the headgroup layer in the sVS bilayers than in the sOS ones, and a smearing effect due to larger fluctuations/defects in the former case. Moreover, from EDPs we could derive the bilayer thickness d_{hh}. For pure PC-PE deposited by sVS, its d_{hh} is considerably larger than pure PC-PE by sOS (41.75 *vs* 38.50 Å). Secondly, the reconstitution of single SNAREs (ΔN in this case) slightly increases d_{hh} (from 41.75 to 43.55 Å), as expected. Lastly for the PC-PE/ΔN + Syb multibilayer (purple), d_{hh} further increases to 49.58 Å, resulting in extremely swelled bilayers. It could possibly originate from the coupling effect between ΔN and Syb. In this case the fully assembled SNARE complex with the 4-helix bundle has to be accommodated into the multilamellar structure, leading to significant structural changes in the host membrane. Nonetheless, at this point we cannot propose any 3d structure to fully clarify our observation. Note that the local lamellar d-spacing around the reconstituted proteins will certainly deviate from the average value probed by reflectivity, which is dominated by membrane area without proteins.

Fig. 4d illustrates the bilayer periodicities *d* derived from the positions of the Bragg peaks, as exampled in Fig. 4c. Unlike the EDPs which can be only obtained at the lamellar RHs, *d* unveils the bilayer structure at all hydration conditions. We can see that (i) *d* of pure PC-PE prepared by sVS is larger than pure PC-PE prepared by sOS, (ii) *d* plots of pure PC-PE and PC-PE/ΔN almost overlap, and (iii) *d* increases significantly in the presence of both ΔN and Syb.

3.4. Grazing-incidence small-angle scattering

Fig. 5 shows the synchrotron (ID01, ESRF) GISAXS patterns of PC-PE-PS-Chol 5:2:2:1 (upper) and PC-PE 4:1 (lower) multibilayers recorded at RH 90% and 95%, respectively. The upper row shows the results of the PC-PE-PS-Chol mixture: (left) pure lipid bilayers prepared by sOS, (center) pure lipid bilayers prepared by sVS, and (right) the lipid bilayers containing both ΔN and Syb prepared by sVS. The typical multilamellar GISAXS patterns with equidistant diffuse Bragg peaks indicate highly aligned and well ordered single lamellar (*L*) phase for all three preparations. The arc like extensions around the sharp Bragg peaks are typically about two orders of magnitude weaker in intensity, representing defects in an otherwise perfectly ordered multilamellar phase. Moreover, we observe a higher number of Bragg peaks in sOS multibilayers than in sVS multibilayers, indicating a higher degree of long range translational order, in good agreement with the reflectivity results. Despite the more pronounced defect level and the associated strain fields, multibilayers prepared by sVS still show high orientation (indicated by the arcs) and long range order, characteristic for the smectic membranes with flat boundaries [14]. GISAXS patterns of PC-PE mixtures are shown in the lower row: (left) pure lipid bilayers by sVS, (center) bilayers containing both ΔN and Syb by sVS, and (right) bilayers prepared by sVS, with ΔN and Syb already mixed before the preparation of proteomicelles and proteoliposomes (referred as premixed hereafter). Similarly to the first lipid mixture, PC-PE multibilayers prepared by sVS also exhibit a single *L* phase, with sufficiently high bilayer orientation and long range order. However, for the premixed sample, two coexisting phases are observed, evidencing clear phase separation. In this preparation, we can assume that the full SNARE complex has been formed from the start and reconstituted via the micelle-vesicle-multibilayer pathway. Hence, the four-helix bundle is anchored via both transmembrane anchors in the same bilayer. Since this presumingly extends the inter-bilayer distance to an unfavorable value, the system seems to react by phase separation. Such a “kinetically or thermodynamically improbable conformation” [57] is also one of the central concerns in the study of membrane proteins. This result is in contrast to the sVS preparation, where the two proteoliposome suspensions are not mixed until right before deposition, which then yields a single phase. With this knowledge, we now start to investigate the phase diagram, in particular extended towards low hydration conditions. To this end, we make use of our in-house instrumentation, for reasons of higher availability compared with synchrotron beamtime.

Fig. 6 shows the in-house GISAXS patterns of PC-PE 4:1 multibilayers of (row 1) pure PC-PE prepared by sOS, (row 2) pure PC-PE prepared by sVS, (row 3) PC-PE with ΔN prepared by sVS, and (row 4) PC-PE with both ΔN and Syb prepared by sVS, measured as a function of RH (50–90 %). The first row shows the familiar *L*-*R* phase transition, in agreement with previous studies of multibilayer lipid stacks [28,35]. The hallmark of the *R* phase are the two off-axis peaks, which are visible in the GISAXS pattern at RH ≤ 60%. With this information at hand, we turn to the sVS samples. In the ideal case, the measured phase diagram should be an intrinsic property of the lipid mixture, not of the preparation. However, this turns out not to be the case. In contrast to the sOS samples on which single phase is always observed, we obtain a pronounced phase-coexistence regime at lower RHs form sVS multibilayers. Furthermore, neither of the two phases transform into the *R* phase when the RH further decreases, even in the presence of both ΔN and Syb. The first *L* phase persists while the second *L* phase transforms into the H_{II} phase. One may speculate whether the difference in the phase diagram, in particular the appearance of the H_{II} phase instead of the *R* phase, can be attributed to the higher defect level in the sVS preparation. While the influence of defects on the phase diagram in soft condensed matter [58] is not completely implausible, we rather believe that this unexpected and complex phase behavior originates from remaining n-OG introduced by the preparation, which has already been evidenced by the comparison of pure vesicles prepared by sonication and by size-exclusion in the SAXS section. Moreover, the structure of the second phase appears to be rather irregular if we compare the three sVS samples, perhaps due to the random concentration of remaining n-OG.

In order to shed more light on this issue, we performed further purification steps of extra column washing and additional dialysis. Fig. 7 presents the comparison of the corresponding GISAXS patterns of PC-PE 1:1 multibilayers, all recorded at RH 50%. The standard purification process consists of a run through a column equilibrated with buffer (to remove detergents), followed by a run through a column equilibrated with ultrapure water (to remove salts) [30], i.e. two runs in total. Its diffraction pattern (Fig. 7 left) exhibits a coexistence of a lamellar phase and a strange 12-fold symmetric quasi-crystal phase [59,60]. Such a phase is rather uncommon for pure lipid systems and can only be attributed to nOG residues in the multibilayer. We then prepared the multibilayer with two extra column runs by repeating the standard purification process, i.e. four runs in total. The corresponding diffraction pattern (Fig. 7 middle) shows a coexistence of two inverted hexagonal phases, rather than the expected coexistence of one inverted hexagonal phase and one rhombohedral (stalk) phase at RH 50% for PC:PE 1:1 [46]. Therefore, we moved one step further and performed additional dialysis on the vesicle suspension after four column runs. To this end, the vesicle suspension was placed in a dialysis bag immersed in 4–5 L of ultrapure water containing 2 mg/L Bio-beads (SM-2 Resin, BIO-RAD). The bath was exchanged every 24 h for three times. Finally, the anticipated stalk phase appeared, as indexed in black in Fig. 7

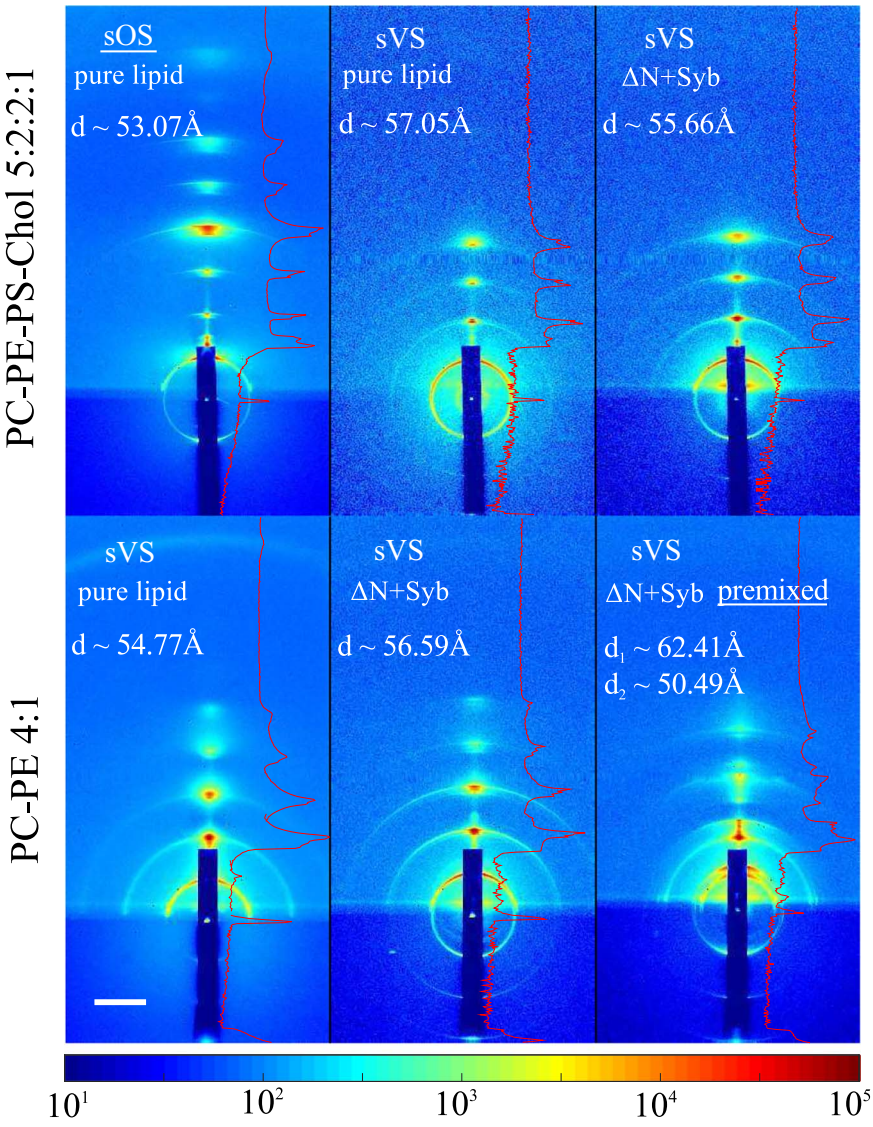

Fig. 5. Upper: Synchrotron GISAXS patterns of multibilayers of (left) pure PC-PE-PS-Chol 5:2:2:1 prepared by sOS, (center) pure PC-PE-PS-Chol 5:2:2:1 prepared by sVS, and (right) PC-PE-PS-Chol 5:2:2:1 containing both ΔN and Syb prepared by sVS. Samples were measured at RH 90%. Lower: Synchrotron GISAXS patterns of sVS multilamellar bilayers of (left) pure PC-PE 4:1, (center) PC-PE 4:1 containing both ΔN and Syb, and (right) PC-PE 4:1 containing both ΔN and Syb where the SNAREs were mixed before the formation of proteomicelles. Samples were measured at RH 95%. The dark blue bar in all images results from the rectangular beamstop. All images were recorded with 10 s exposure time with the specular beam lying between the primary beam and 1st Bragg peak behind the beamstop. Each exposure is normalized by its total intensity. The intensity profiles along the $q_{\|} = 0$ direction are plotted in red. The *d* values in the images represent the bilayer periodicities, and the white scale bar in the lowerleft corner indicates 50 pixels on the detector. The false color scale corresponds to the logarithmic scattering intensity.

(right). Such a coexistence of one hexagonal phase and one rhombohedral phase agrees perfectly with our previous observation on sOS multibilayers [46]. This result clearly demonstrates that the standard purification procedure cannot sufficiently remove the detergents for meaningful phase diagram studies.

4. Conclusion

In this study we have extended the vesicle-based SNARE reconstitution from supported single bilayers to supported lipid bilayer stacks. In the novel protocol, the t-SNARE (ΔN) and v-SNARE (Syb) were first separately reconstituted into micelles and then vesicles. Afterwards vesicles containing the t-SNARE and v-SNARE were mixed, incubated prior to deposition onto the substrate, where H_2O was removed by evacuation to yield highly oriented supported multibilayers. The proteomicelles and proteoliposomes were characterized by SAXS, and the final supported lipid multibilayers by X-ray reflectivity and GISAXS, depicting a complete pathway (Fig. 1b) for the reconstitution of proteins into supported bilayer stacks.

The SAXS and reflectivity experiments reveal that (i) the sVS method can also yield well aligned bilayer stacks with sufficient long-range order for X-ray study and for EDP reconstruction despite substantial defects caused by incomplete vesicle rupture; (ii) the reconstitution of single SNAREs does not dramatically alter the structure of neither the micelles, nor the vesicles, nor the resulting multibilayers; (iii) ΔN and Syb together lead to a significant structural alteration of the multibilayer and to a decrease in lamellar ordering. In addition, GISAXS results of the sVS multibilayers show that at higher RHs a single *L* phase is preserved also in the presence of SNAREs, i.e. no micro-phase separation occurs. Contrarily, at lower RHs a two-state coexistence appears, with neither of the two phases being the expected stalk (*R*) phase. This unexpected phase behavior was observed for SNARE containing as well as for protein-free sVS multibilayers, and was attributed to residual detergents. Only after extended dialysis carried out over three days, the stalk phase appeared in the sVS samples. Hence we can conclude that residual detergents induce additional phases and inhibit the $L-R$ phase transition, and that standard column purification and overnight dialysis is not sufficient. For this reason, our goal to establish the phase diagram for SNARE containing lipid bilayers cannot be easily achieved. Future efforts should be directed at identifying detergents which can be removed more easily and more effective purification steps [61]. Notwithstanding future improvements of the protocol, indirect characterization of SNAREs in the multibilayers prepared by the novel protocol is however, already possible at the present stage, in particular in the lamellar state.

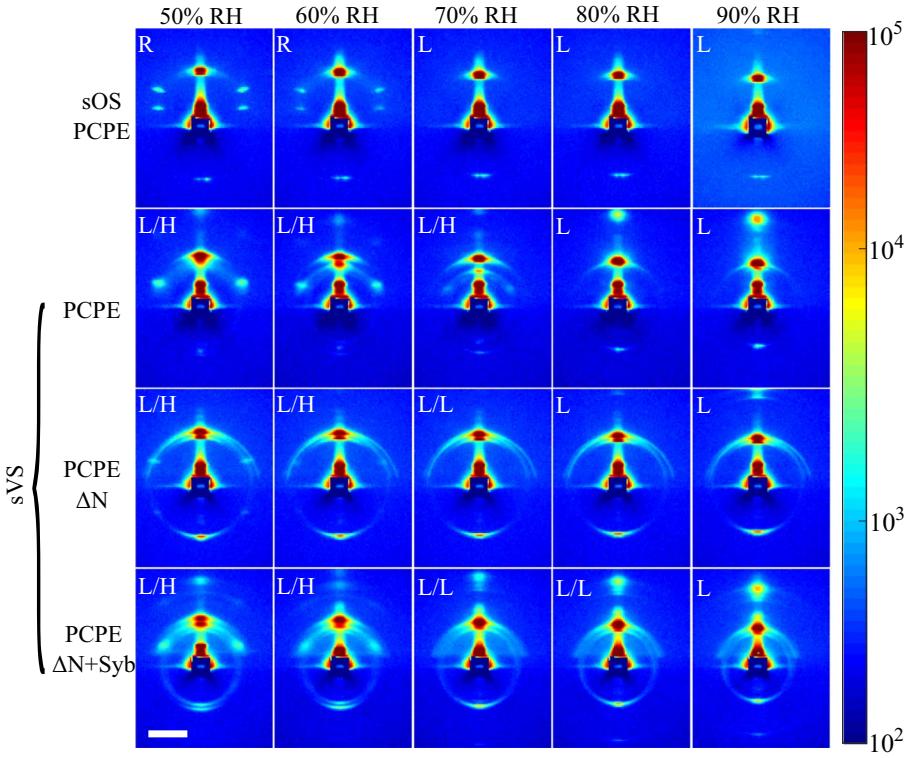

Fig. 6. In-house GISAXS patterns of multibilayers of (row 1) pure PC-PE 4:1 prepared by sOS, (row 2) pure PC-PE 4:1 prepared by sVS, (row 3) PC-PE 4:1 reconstituted with ΔN prepared by sVS and (row 4) PC-PE 4:1 containing both ΔN and Syb prepared by sVS, measured at various hydration conditions (RH 50–90%). All samples were exposed for 1000 s with the incidence angle $\theta \approx 0.3^{\circ}$. The bilayer phases determined in combination with the reflectivity data, are denoted in the upper left corner of each image, and the white scale bar in the lower left corner indicates 20 pixels on the detector. The shadow in the center results from the square-shape beamstop. The pseudo color scale corresponds to the logarithmic scattering intensity.

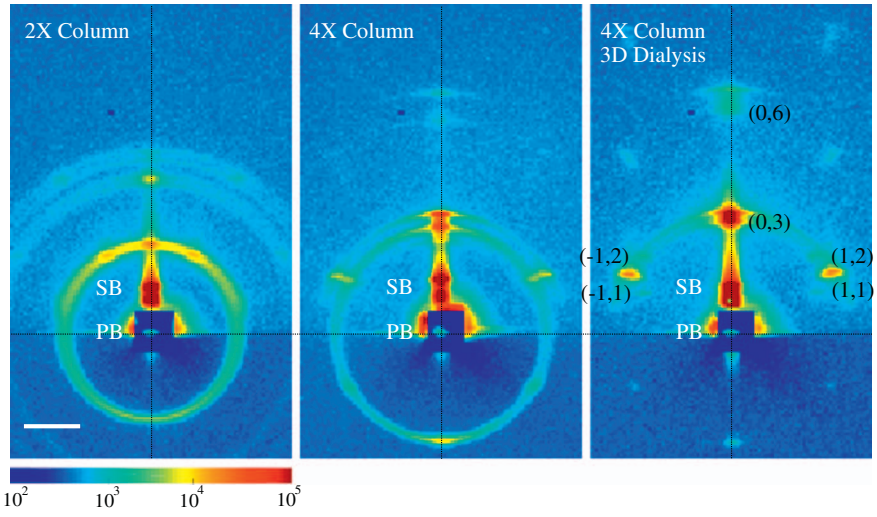

Fig. 7. (left) In-house GISAXS pattern of PC-PE 1:1 multibilayers prepared by sVS with standard purification. The lipid/protein suspensions passed through the column two times in total. (middle) In-house GISAXS pattern of PC-PE 1:1 multibilayers prepared by sVS with extra purification. The lipid/protein suspensions passed through the column four times in total. (right) In-house GISAXS pattern of PC-PE 1:1 multibilayers prepared by sVS with extra purification. After four column runs, the lipid/protein suspensions was dialysized against pure water with Biobeads for 3 days. All samples were exposed for 1000 s at RH 50% at incidence angle $\theta \approx 0.4^{\circ}$. The primary beam (PB) and specular beam (SB) are denoted in white. The rhombohedral indices are denoted in black. The white scale bar in the lower left corner indicates 20 pixels on the detector. The false color scale corresponds to the logarithmic scattering intensity. The shadow in the center of each pattern results from the square-shape beamstop.

Transparency document

The Transparency document associated with this article can be found, in online version.

Acknowledgments

The authors acknowledge the European Synchrotron Radiation Facility for provision of synchrotron radiation facilities and we thank Jan Hilhost for assistance in using beamline ID01. We acknowledge Partnership for Soft Condensed Matter (PSCM) at ESRF for allowing us to use their laboratory for sample preparation, and Annalena Salditt for the help with SAXS experiments. We also thank Susanne Hengst for her kind assistance with the sample preparation, Sebastian Äffner for his help with the manuscript and the German Science Foundation DFG (SFB 803) for the financial support.

Appendix A. Estimation of N_{SNARE} per micelle

To better interpret the presence or absence of changes in the SAXS measurements with SNARE reconstitution, it is essential to first estimate the average SNARE number per micelle, since the SAXS measurements correspond to an ensemble average (see the discussion in the main text). Below we present the parameters used in the corresponding calculation, i.e. SAXS results in Table 1a for the micelle geometry, literature values for lipid and surfactants [34,50] and the stoichiometry parameters of our preparation. We conclude that only 9% of all micelles have a reconstituted SNARE protein. Contrarily, for vesicles the average copy number of SNARE is significantly larger than one, namely ~ 44 (see Appendix C).

List of constants[1]

V_{nOG}[Å^3]	243	volume per nOG molecule
V_{lipid}[Å^3]	1620	volume per lipid molecule
M_{nOG} [g/mol]	282	molecular mass of nOG
M_{lipid} [g/mol]	876	molecular mass of the lipid
CMC [mg/ml]	6.08	critical micelle concentration of nOG
m_{nOG} [g]	1.80	mass of nOG
m_{lipid} [g]	1.00	mass of the lipid
$V_{solution}$[μL]	0.07	volume of the micelle suspension
a [Å]	11.87	fitted polar radius of Syb proteomicelles
b [Å]	31.40	fitted equatorial radius of Syb proteomicelles
t_a [Å]	12.59	fitted polar shell thickness
t_b [Å]	2.71	fitted equatorial shell thickness
$R_{protein/lipid}$	1:500	protein/lipid molar ratio

Calculation

$$V_{\text{micelle}} = \frac{4}{3}\pi(a + t_a)(b + t_b)^2 \approx 119209 \text{ Å}^3 \tag{A.1}$$

$$R_{\text{lipid/nOG}} = \frac{m_{\text{lipid}}/M_{\text{lipid}}}{(m_{nOG} - V_{\text{solution}}{\cdot}CMC)/M_{\text{nOG}}} \approx 0.27 \tag{A.2}$$

$$N_{\text{nOG}} = \frac{V_{\text{micelle}}}{V_{\text{nOG}} + V_{\text{lipid}}R_{\text{lipid/nOG}}} \approx 175 \tag{A.3}$$

$$N_{\text{SNARE}} = N_{\text{nOG}}R_{\text{lipid/nOG}}R_{\text{protein/lipid}} \approx 0.09 \tag{A.4}$$

Appendix B. Dynamic light scattering results of vesicles

Dynamic Light Scattering was carried out to gain the size distribution of various vesicles, in particular the ΔN-reconstituted proteoliposomes. Thus the effect of SNARE-reconstitution on vesicle size and ΔN-induced vesicle aggregation could be evaluated.

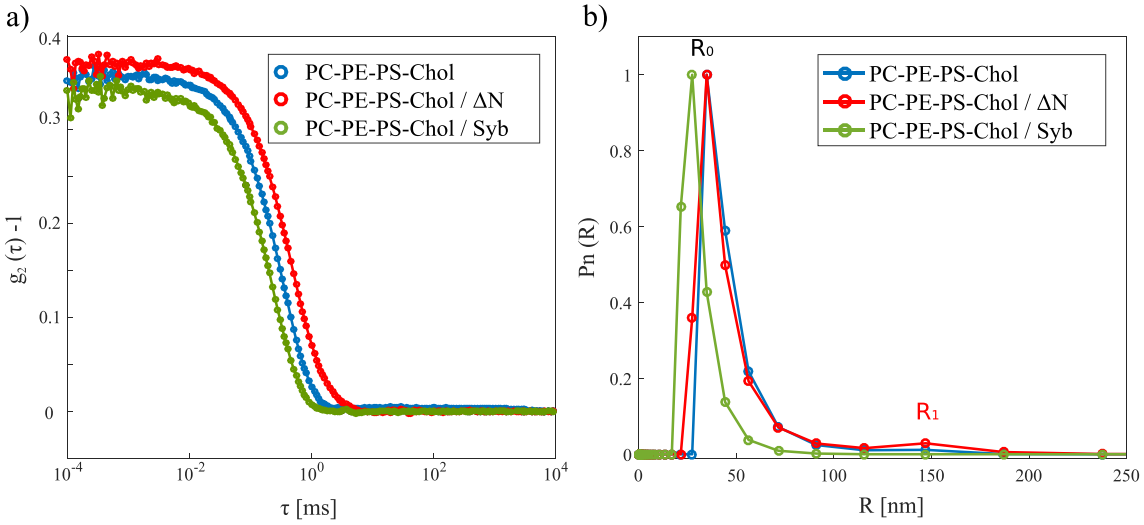

Fig. B.1. (a) DLS correlation curves and (b) vesicle size distributions of (i) pure PC-PE-PS-Chol, (ii) PC-PE-PS-Chol/ΔN and (iii) PC-PE-PS-Chol/Syb prepared by the column method. Measurements were carried out on ALV/CGS-3 laser light scattering goniometer system (ALG-Gmbh, Langen, Germany), equipped with a 22 mW HeNe laser (λ = 632.8 nm) at 90° scattering angle. Logarithmic number-weighting was carried out for the fitting. All three vesicles share a mean radius $R_0 \approx 30$ nm, with ΔN bringing about a unique R_1 around 150 nm probably due to protein aggregation. Vesicles suspensions were diluted to ~0.01 mg/mL for DLS study.

Appendix C. Estimation of N_{SNARE} per vesicle

Similar to the estimation in Appendix A, we have performed a calculation of the copy number N_{SNARE} per vesicle. Below we present the calculation using parameters obtained from literature [50], SAXS results in Table 1b and DLS results in Appendix B.

[1] Parameters of DOPC rather than the lipid mixtures are used.

List of constants[2]

V_{lipid}[Å^3]	1620	volume per lipid molecule
R_0[Å]	300	mean vesicle radius from DLS
Db [Å]	36.76	bilayer thickness from SAXS fitting
$R_{protein/lipid}$	1:500	protein/lipid molar ratio

Calculation

$$V_{out} = \frac{4}{3}\pi R_0^3 \approx 1.13 \times 10^8 \text{ Å}^3 \quad (C.1)$$

$$V_{in} = \frac{4}{3}\pi (R_0 - Db)^3 \approx 7.64 \times 10^7 \text{ Å}^3 \quad (C.2)$$

$$N_{SNARE} = \frac{V_{out} - V_{in}}{V_{lipid}} R_{protein/lipid} \approx 43.61 \quad (C.3)$$

Appendix D. Fitting vesicle SAXS data with different models and choice of cut-off parameter

For the fitting of vesicle SAXS data, several alternative models can be used. Using the spherical model [41,42], the entire q-range can be fitted and the radius R as well as the polydispersity σ_R can be retrieved. However, as shape fluctuations and structure factor effects (due to aggregation of vesicles) are not included, it is sometimes more challenging to extract the bilayer profiles in such a full model. Contrarily, a simple and robust alternative is to use the flat (powder-averaged) bilayer model, which retrieves the profile ρ(z) from the high-q data, excluding low-q data from the fit. To justify the choice of the cut-off, we present a comparison of the flat bilayer model and the spherical model in Fig. D.1. Results show that not only can both model adequately describe the SAXS data, but also yield comparable bilayer thickness d_{hh} and electron density contrast ρ_1 (see the legend of Fig. D.1). Note, however, that the standard deviation σ of the 3-Gaussian model deviate. Since the second form factor maximum is better captured by the flat bilayer model, and the spherical model in addition is systematically too low at low-q, we favor the flat bilayer model with the cut-off at 0.075 Å^{-1}, as indicated by the vertical dashed line.

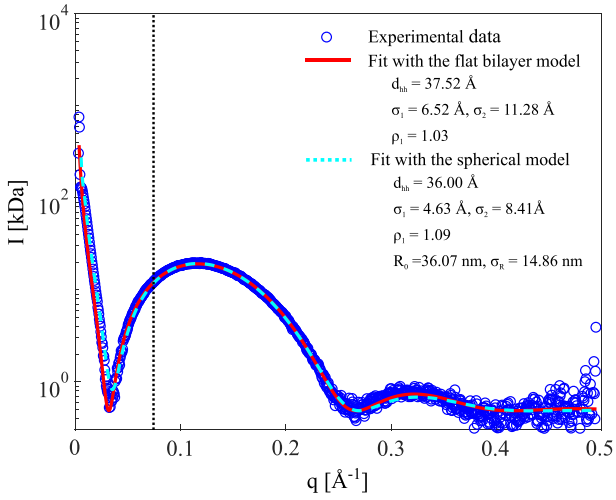

Fig. D.1. The experiment SAXS curve (blue circles), fit with the flat bilayer model (red solid line) and fit with the spherical model (cyan dashed line) of PC-PE-PS-Chol 5:2:2:1 vesicles prepared by sonication. The fitting results of both models are shown in the legend. The vertical dashed line indicates the cutoff for the flat bilayer model. Fitting is performed in the q range of 0.075–0.495 Å^{-1} for the flat bilayer model and over the full q range for the spherical model. The resulting bilayer thickness d_{hh} for the two models, i.e. 37.52 and 36.00 Å, respectively, and the maximum electron density contrast of the headgroup region ρ_1, i.e. 1.03 and 1.09 (a.u.), respectively, differ only slightly.

References

[1] R. Jahn, R.H. Scheller, SNAREs: engines for membrane fusion, Nat. Rev. Mol. Cell Biol. 7 (2006) 631–643.
[2] T.C. Suedhof, J.E. Rothman, Membrane fusion: grappling with SNARE and SM proteins, Science 323 (5913) (2009) 474–477.
[3] P.I. Hanson, J.E. Heuser, R. Jahn, Neurotransmitter release - four years of SNARE complexes, Curr. Opin. Neurobiol. 7 (1997) 310–315.
[4] Y.A. Chen, R.H. Scheller, SNARE-mediated membrane fusion, Nat. Rev. Mol. Cell Biol. 2 (2001) 98–106.
[5] J. Katsaras, T. Gutberlet, Lipid Bilayers: Structure and Interactions, Springer Science & Business Media, 2013.
[6] M. Winterhalter, Black lipid membranes, Curr. Opin. Colloid Interface Sci. 5 (2000) 250–255.
[7] J. Wilschut, D. Hoekstra, Special issue: liposomes membrane fusion: lipid vesicles as a model system, Chem. Phys. Lipids 40 (1986) 145–166.
[8] A. Nath, W.M. Atkins, S.G. Sligar, Applications of phospholipid bilayer nanodiscs in the study of membranes and membrane proteins, Biochemistry 46 (2007) 2059–2069.
[9] E. Sackmann, Supported membranes: scientific and practical applications, Science 271 (1996) 43.
[10] E. Novakova, G. Mitrea, C. Peth, J. Thieme, K. Mann, T. Salditt, Solid supported multicomponent lipid membranes studied by X-ray spectromicroscopy, Biointerphases 3 (2008) 44–54.
[11] M. Kornreich, R. Avinery, R. Beck, Modern X-ray scattering studies of complex biological systems, Curr. Opin. Biotechnol. 24 (2013) 716–723.
[12] P. Heftberger, B. Kollmitzer, F.A. Heberle, J. Pan, M. Rappolt, H. Amenitsch, N.

[2] Parameters of DOPC rather than the lipid mixtures are used.

Kucerka, J. Katsaras, G. Pabst, Global small-angle X-ray scattering data analysis for multilamellar vesicles: the evolution of the scattering density profile model, J. Appl. Crystallogr. 47 (2013) 173–180.
[13] E. Novakova, K. Giewekemeyer, T. Salditt, Structure of two-component lipid membranes on solid support: an X-ray reflectivity study, Phys. Rev. E 74 (2006) 051911.
[14] D. Constantin, U. Mennicke, C. Li, T. Salditt, Solid-supported lipid multilayers: structure factor and fluctuations, Eur. Phys. J. E 12 (2003) 283–290.
[15] S. Himbert, R.J. Alsop, M. Rose, L. Hertz, A. Dhaliwal, J.M. Moran-Mirabal, C.P. Verschoor, D.M.E. Bowdish, L. Kaestner, C. Wagner, M.C. Rheinstädter, The molecular structure of human red blood cell membranes from highly oriented, solid supported multi-lamellar membranes, Sci. Rep. 7 (2017) 39661.
[16] T. Salditt, C. Li, A. Spaar, U. Mennicke, X-ray reflectivity of solid-supported multilamellar membranes, Eur. Phys. J. E 7 (2002) 105.
[17] L. Yang, L. Ding, H.W. Huang, New phases of phospholipids and implications to the membrane fusion problem, Biochemistry 42 (2003) 6631–6635.
[18] N. Kucerka, J. Pencer, J.N. Sachs, J.F. Nagle, J. Katsaras, Curvature effect on the structure of phospholipid bilayers, Langmuir 23 (2007) 1292–1299.
[19] E.-K. Sinner, W. Knoll, Functional tethered membranes, Curr. Opin. Chem. Biol. 5 (2001) 705–711.
[20] M. Seul, M. Sammon, Preparation of surfactant multilayer films on solid substrates by deposition from organic solution. Thin Solid Films 185 (1990) 287.
[21] L.K. Tamm, S.A. Tatulian, Infrared spectroscopy of proteins and peptides in lipid bilayers, Q. Rev. Biophys. 30 (1997) 365–429.
[22] E. Goormaghtigh, V. Cabiaus, J.-M. Ruysschaert, Secondary structure and dosage of soluble and membrane proteins by attenuated total reflection Fourier-transform infrared spectroscopy on hydrated films, Eur. J. Biochem. 193 (1990) 420.
[23] A.A. Brian, H.M. McConnell, Allogeneic stimulation of cytotoxic T cells by supported planar membranes, Proc. Natl. Acad. Sci. U. S. A. 81 (1984) 6159–6163.
[24] V. Kiessling, L.K. Tamm, Measuring distances in supported bilayers by fluorescence interference-contrast microscopy: polymer supports and SNARE proteins, Biophys. J. 84 (2003) 408–418.
[25] D.E. Saslowsky, J.C. Lawrence, R.M. Henderson, J.M. Edwardson, Syntaxin is efficiently excluded from Sphingomyelin-enriched domains in supported lipid bilayers containing cholesterol, J. Membr. Biol. 194 (2003) 153–164.
[26] N. Kucerka, E. Dushanov, K.T. Kholmurodov, J. Katsaras, D. Uhrikova, Calcium and zinc differentially affect the structure of lipid membranes, Langmuir 33 (2017) 3134–3141.
[27] L. Yang, H.W. Huang, Observation of a membrane fusion intermediate structure, Science 297 (2002) 1877–1879.
[28] S. Aeffner, T. Reusch, B. Weinhausen, T. Salditt, Energetics of stalk intermediates in membrane fusion are controlled by lipid composition, Proc. Natl. Acad. Sci. U. S. A. 109 (2012) E1609–E1618.
[29] A.V. Pobbati, A. Stein, D. Fasshauer, N- to C-terminal SNARE complex assembly promotes rapid membrane fusion, Science 313 (2006) 673–676.
[30] L.L.G. Schwenen, R. Hubrich, D. Milovanovic, B. Geil, J. Yang, A. Kros, R. Jahn, C. Steinem, Resolving single membrane fusion events on planar pore-spanning membranes, Sci. Rep. 5 (2015) 12006.
[31] J.W. Kuhlmann, M. Junius, U. Diederichsen, C. Steinem, SNARE-mediated single-vesicle fusion events with supported and freestanding lipid membranes, Biophys. J. 112 (2017) 2348–2356.
[32] A. Stein, A. Radhakrishnan, D. Riedel, D. Fasshauer, R. Jahn, Synaptotagmin activates membrane fusion through a Ca2+-dependent trans interaction with phospholipids, Nat. Struct. Mol. Biol. 14 (2007) 904–911.
[33] M. Ollivon, S. Lesieur, C.G. Madelmont, M. Paternostre, Vesicle reconstitution from lipid-detergent mixed micelles, BBA-Biomembranes 1508 (2000) 34–50.
[34] M.R. Wenk, T. Alt, A. Seelig, J. Seelig, Octyl-beta-D-glucopyranoside partitioning into lipid bilayers: thermodynamics of binding and structural changes of the bilayer. Biophys. J. 72 (1997) 1719–1731.
[35] Z. Khattari, S. Köhler, Y. Xu, S. Aeffner, T. Salditt, Stalk formation as a function of lipid composition studied by X-ray reflectivity, BBA - Biomembranes 1848 (2015) 41–50.
[36] P. Pernot, A. Round, R. Barrett, A. De Maria Antolinos, A. Gobbo, E. Gordon, J. Huet, J. Kieffer, M. Lentini, M. Mattenet, C. Morawe, C. Mueller-Dieckmann, S. Ohlsson, W. Schmid, J. Surr, P. Theveneau, L. Zerrad, S. McSweeney, Upgraded ESRF BM29 beamline for SAXS on macromolecules in solution, J. Synchrotron Rad. 20 (2013) 660–664.
[37] M.F. Incardona, G.P. Bourenkov, K. Levik, R.A. Pieritz, A.N. Popov, O. Svensson, EDNA: a framework for plugin-based applications applied to X-ray experiment online data analysis, J. Synchrotron Rad. 16 (2009) 872–879.
[38] M.E. Brennich, J. Kieffer, G. Bonamis, A. De Maria Antolinos, S. Hutin, P. Pernot, A. Round, Online data analysis at the ESRF bioSAXS beamline, BM29, J. Appl. Crystallogr. 49 (2016) 203–212.
[39] J. Lipfert, L. Columbus, V.B. Chu, S.A. Lesley, S. Doniach, Size and shape of detergent micelles determined by small-angle X-ray scattering, J. Phys. Chem. B 111 (2007) 12427–12438.
[40] R.C. Oliver, J. Lipfert, D.A. Fox, R.H. Lo, S. Doniach, L. Columbus, Dependence of micelle size and shape on detergent alkyl chain length and head group, PLoS One 8 (2013) e62488.
[41] M.R. Brzustowicz, A.T. Brunger, X-ray scattering from unilamellar lipid vesicles, J. Appl. Crystallogr. 38 (2005) 126–131.
[42] P. Székely, A. Ginsburg, T. Ben-Nun, U. Raviv, Solution X-ray scattering form factors of supramolecular self-assembled structures, Langmuir 26 (2010) 13110–13129.
[43] G. Pabst, M. Rappolt, H. Amenitsch, P. Laggner, Structural information from multilamellar liposomes at full hydration: full q-range fitting with high quality X-ray data, Phys. Rev. E 62 (2000) 4000–4009.
[44] S. Aeffner, T. Reusch, B. Weinhausen, T. Salditt, Membrane fusion intermediates and the effect of cholesterol: an in-house X-ray scattering study, Eur. Phys. J. E 30 (2009) 204–214.
[45] H.W. Huang, W. Liu, G.A. Olah, Y. Wu, Physical techniques of membrane studies - study of membrane active peptides in bilayers, Prog. Surf. Sci. 38 (1991) 145–199.
[46] S. Aeffner, Stalk Structures in Lipid Bilayer Fusion Studied by X-ray Diffraction, Ph.D. thesis Institute for X-ray Physics, Georg-August University Goettingen, 2011.
[47] G.V. Jensen, R. Lund, J. Gummel, M. Monkenbusch, T. Narayanan, J.S. Pedersen, Direct observation of the formation of surfactant micelles under nonisothermal conditions by synchrotron SAXS, J. Am. Chem. Soc. 135 (2013) 7214–7222.
[48] J. Lipfert, S. Doniach, Small-angle X-ray scattering from RNA, proteins, and protein complexes, Annu. Rev. Biophys. Biomol. Struct. 36 (2007) 307–327.
[49] M. Ollivon, O. Eidelman, R. Blumenthal, A. Walter, Micelle-vesicle transition of egg phosphatidylcholine and octyl glucoside, Biochemistry 27 (1988) 1695–1703.
[50] S. Almog, B. Litman, W. Wimley, J. Cohen, E. Wachtel, Y. Barenholz, A. Ben-Shaul, D. Lichtenberg, States of aggregation and phase transformations in mixtures of phosphatidylcholine and octyl glucoside, Biochemistry 29 (1990) 4582–4592.
[51] E. Mylonas, D.I. Svergun, Accuracy of molecular mass determination of proteins in solution by small-angle X-ray scattering, J. Appl. Crystallogr. 40 (2007) s245–s249.
[52] R. Zhang, P.A. Marone, P. Thiyagarajan, D.M. Tiede, Structure and molecular fluctuations of n-alkyl-β-D-glucopyranoside micelles determined by X-ray and neutron scattering, Langmuir 15 (1999) 7510–7519.
[53] J. Lasch, J. Hoffman, W.G. Omelyanenko, A.A. Klibanov, V.P. Torchilin, H. Binder, K. Gawrisch, Interaction of Triton X-100 and octyl glucoside with liposomal membranes at sublytic and lytic concentrations. Spectroscopic studies, BBA - Biomembranes 1022 (1990) 171–180.
[54] B. Angelov, M. Ollivon, A. Angelova, X-ray diffraction study of the effect of the detergent octyl glucoside on the structure of lamellar and nonlamellar lipid/water phases of use for membrane protein reconstitution, Langmuir 15 (1999) 8225–8234.
[55] R.P. Richter, R. Bérat, A.R. Brisson, Formation of solid-supported lipid bilayers: an integrated view, Langmuir 22 (2006) 3497–3505.
[56] J. Nagle, R. Zhang, S. Tristram-Nagle, W. Sun, H. Petrache, R. Suter, X-ray structure determination of fully hydrated L alpha phase dipalmitoylphosphatidylcholine bilayers, Biophys. J. 70 (1996) 1419–1431.
[57] L. Silvestro, P.H. Axelsen, Infrared spectroscopy of supported lipid monolayer, bilayer, and multibilayer membranes, Chem. Phys. Lipids 96 (1998) 69–80.
[58] D.R. Nelson, Defects and Geometry in Condensed Matter Physics, Cambridge University Press, 2002.
[59] X. Zeng, G. Ungar, Y. Liu, V. Percec, A.E. Dulcey, J.K. Hobbs, Supramolecular dendritic liquid quasicrystals, Nature 428 (2004) 157–160.
[60] Y. Feng, D. Rainteau, C. Chachaty, Z.-W. Yu, C. Wolf, P.J. Quinn, Characterization of a quasicrystalline phase in codispersions of phosphatidylethanolamine and glucocerebroside, Biophys. J. 86 (2004) 2208–2217.
[61] A.M. Seddon, P. Curnow, P.J. Booth, Membrane proteins, lipids and detergents: not just a soap opera, BBA - Biomembranes 1666 (2004) 105–117.